Tin oxide light-scattering layer for Titania Photoanodes in dye-sensitized solar cells

SnO_2 Light Scattering Layer for TiO_2 Photoanode in Dye-Sensitized Solar Cells

Munkhbayar Batmunkh,[a, b] Mahnaz Dadkhah,[b] Cameron J. Shearer,[b] Mark J. Biggs,[a, c] and Joseph G. Shapter*[b]

Dedication ((optional))

Abstract: High-performance dye-sensitized solar cell (DSSC) devices rely on photoanodes that possess excellent light-harvesting capability and high surface area for sufficient dye adsorption. In this work, morphologically controlled SnO_2 microstructures have been synthesized and used as an efficient light backscattering layer on top of the nanocrystalline TiO_2 layer to prepare a double-layered photoanode. By optimizing the thickness of both the TiO_2 bottom layer and SnO_2 top layer, a high power conversion efficiency (PCE) of 7.8% is achieved, demonstrating a ~38% enhancement in the efficiency when compared to a nanocrystalline TiO_2-only photoanode (5.6%). We attribute this efficiency improvement to the superior light backscattering capability of SnO_2 microstructures.

Introduction

Some ten years ago, the now late Nobel Laureate Richard Smalley was asked to define the world's ten most pressing problems.[1] He provided this list with energy at the top and in fact argued that there was really only one problem suggesting that access to cheap, reliable energy was the key to solving the big issues of the world. This is still true today and has led to an enormous research effort to improve energy efficiencies, develop new energy production methods as well as innovation in energy storage. Recent developments in photovoltaic (PV) technologies, particularly perovskite solar cells (PSCs) and dye-sensitized solar cells (DSSCs), have shown great promise in addressing current energy related issues.[2, 3] Although the significant development that has been made in the PSC efficiencies in a short time is very exciting[4], toxicity and instability of PSCs still present considerable challenges in their commercialization. In contrast to the PSCs, DSSCs possess comparable efficiencies[5] (e.g. ~14%[5]) yet are non-toxic, demonstrate long-term stability, and are simple and cheap to manufacture.[6]

[a] Munkhbayar Batmunkh, Prof. Mark J. Biggs
School of Chemical Engineering
The University of Adelaide
Adelaide, South Australia 5005, Australia

[b] Munkhbayar Batmunkh, Dr. Mahnaz Dadkhah, Dr. Cameron J. Shearer, Prof. Joseph G. Shapter*
School of Chemical and Physical Sciences
Flinders University
Bedford Park, Adelaide, South Australia 5001, Australia
E-mail: joe.shapter@flinders.edu.au

[c] Prof. Mark J. Biggs
School of Science
Loughborough University
Loughborough, Leicestershire, LE11 3TU, UK

Supporting information for this article is given via a link at the end of the document.

There are many excellent reviews of the DSSC field.[7-10] A typical DSSC consists of a working electrode (photoanode) and a counter electrode with an electrolyte sandwiched between. Of particular interest in this report is the photoanode which typically consists of an organic dye adsorbed onto a mesoporous film composed of 10-30 nm semiconducting oxide (usually TiO_2) nanoparticles on a transparent conducting oxide (TCO) substrate. However, these traditional photoanodes demonstrate poor solar light harvesting efficiency in the visible region due to the lack of absorption of incident photons (Figure 1a left side).[11-13] This issue has led many researchers to investigate possible alternative DSSC photoanodes over the years.[12-17]

Double-layered photoanodes made-up of a film composed of smaller (10s of nm) nanoparticles deposited on the TCO and a second layer of larger particles (100s of nm) on top that backscatters the light have been developed to enhance DSSC performance.[18-21] So far, a variety of TiO_2 structures such as hollow spheres,[20, 22] mesopororous beads,[23, 24] hierarchical microsphere,[25-27] mesoporous microspheres,[28] and others[29-32] have been employed in the backscattering layer. In addition to these TiO_2 structures, researchers have explored other alternative backscattering layers (for example ZnO,[33-35] CeO_2,[36] SnO_2,[37-39] and $Y_3Al_5O_{12}$:Ce phosphors[40]) and used them in DSSC photoanodes because of their unique light backscattering capability and high photostability. However, the power conversion efficiency (PCE) enhancements achieved using these light backscatters as compared to their control devices are still unsatisfactory. Interestingly, backscattering films composed of submicrometer-sized SnO_2 particles have recently shown promising improvements in DSSC performance when used with TiO_2 photoanodes.[41-44] Although these studies have shown considerable enhancement in the device efficiency, none have provided a deep understanding of the origins of these improvements. Therefore, a detailed investigation is still needed to fully elucidate the role of SnO_2 light backscattering layers in the DSSC photoanodes.

In the present work, we explore the use of microstructured SnO_2 rods as backscattering layers in DSSCs photoanodes (Figure 1a right side). A double-layered photoanode composed of a SnO_2 microstructure, which offers the potential for efficient light backscattering, on top of a nanocrystalline TiO_2 layer with good dye-loading capacity was designed to produce high-performance DSSCs (Figure 1b). By investigating the thickness of both the SnO_2 and TiO_2 layers of the cells, a significant enhancement in the PCE was observed as compared to the device fabricated without the SnO_2 backscattering layer. The PCE enhancement of DSSC in the presence of the SnO_2 layer is due only to the enhanced light-harvesting efficiency of the photoanode with the microstructured SnO_2.

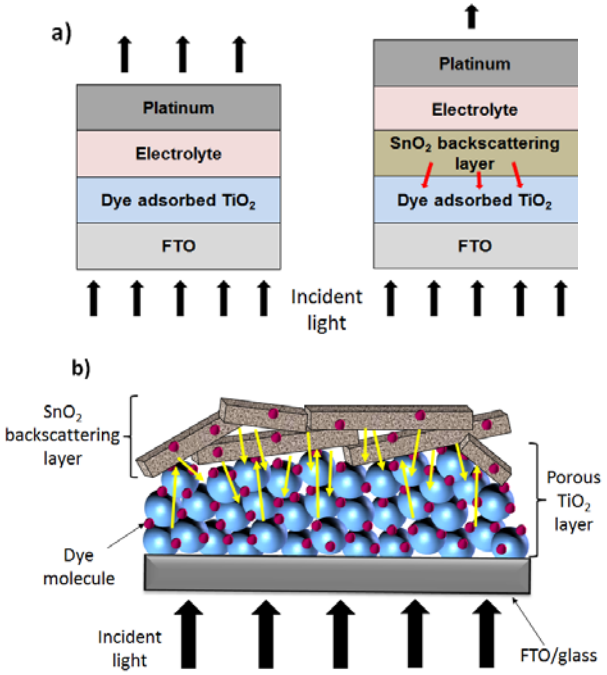

Figure 1. Schematic of (a) DSSC fabricated (left) without and (right) with SnO_2 backscattering layer; and (b) double-layered DSSC photoanode with SnO_2 backscattering layer on top of TiO_2 mesoporous layer.

Results and Discussion

Characterization and photovoltaic performance of the as prepared, microwaved and calcined SnO_2 based DSSCs

The preparation procedure of the as prepared, microwaved and calcined samples is shown in Figure 2a. A detailed description of the process is given in the experimental section. Typically, a $SnCl_2{\cdot}2H_2O$ powder was used as a starting material. It was first mixed with hydrochloric acid (0.02 M) solution before stirring for 45 min. This process leads to the precipitation of SnO_2 rods, which are denoted here "as prepared" SnO_2 (AP-SnO_2). The AP-SnO_2 samples were reacted using a microwave technique for 5 min under 600 W power to give "microwaved" SnO_2 (MW-SnO_2). In order to improve the crystallinity of the SnO_2, the MW-SnO_2 samples were calcined at 500^{o}C for 3 h in air yielding "calcined" SnO_2 (C-SnO_2). These three samples were characterized using X-ray diffraction (XRD), scanning electron microscopy (SEM), and Attenuated Total Reflection-Fourier Transform Infrared Spectroscopy (ATR-FTIR).

XRD patterns of the synthesized samples are shown in Figure 2b. The peaks, assigned to (110), (101), (211), (310) and (312), were observed for all three samples, suggesting that the synthesized structures had various degrees of crystallinity. Particularly, it can be seen that the AP-SnO_2 and MW-SnO_2 structures display very broad and weak peaks, indicative of SnO_2 of poor crystallinity. In contrast, the C-SnO_2 sample shows narrow, strong peaks which can be assigned to a typical tetragonal rutile structure (JCPDS card no. 41-1445), indicative of highly-crystalline SnO_2.[37, 44] The ATR-FTIR spectra of the prepared samples, which are shown in Figure S1, further confirm the XRD results. A high crystallinity and wide band gap, without dopant and defects is favored for backscattering as both have been shown to introduce energy levels between the band gap that allow visible light absorption and luminescence.[45, 46]

Figure 2c-e shows the SEM images of three different SnO_2 structures. The synthesized SnO_2 structures were found to be typically rod shaped with average lengths of about 5 µm and width of about 1.8 µm. As shown in Figure 2c, the AP-SnO_2 sample was strongly aggregated. After treating AP-SnO_2 using the microwave, the strong aggregation was significantly reduced and the length and diameter of SnO_2 micro-rod also decreased (see Figure 2d) by almost 2-fold. As illustrated in Figure 2e, no significant changes in the morphology compared to the MW-SnO_2 samples were observed for the SnO_2 structures after calcination. But as discussed previously, the calcination for SnO_2 is necessary to improve the sample crystallinity.

To explore the effect of different SnO_2 samples on the PV efficiency, DSSC devices were fabricated using AP-SnO_2, MW-SnO_2 and C-SnO_2 on top of TiO_2 as photoanodes and their performances were compared with control cells based on TiO_2-only photoanodes. The bilayer photoanodes were prepared by doctor blading SnO_2 layers on top of ~15.5 µm thick TiO_2 layer. After depositing both TiO_2 and SnO_2 on a FTO electrode, the photoanodes were soaked in N719 dye solution to saturation coverage.

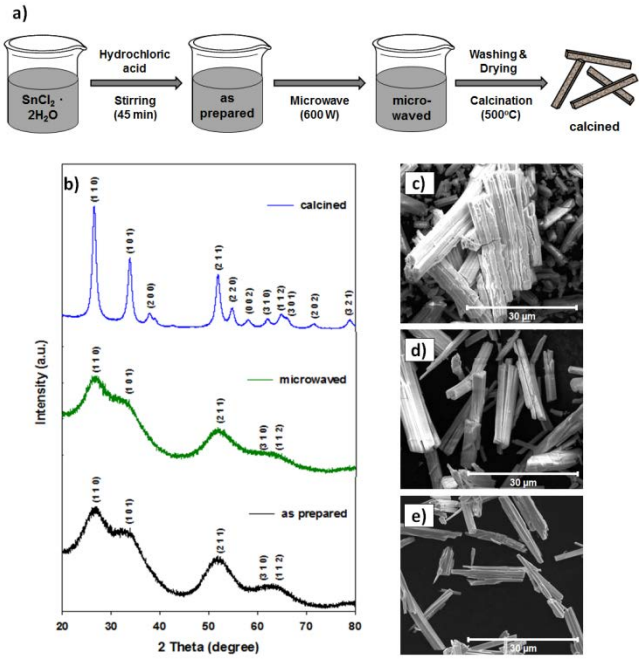

Figure 2 – (a) Schematic for the preparation procedure of the samples, (b) XRD patterns of the synthesized samples and SEM image of (c) as prepared SnO_2 (AP-SnO_2), (d) microwaved SnO_2 (MW-SnO_2) and (e) calcined SnO_2 (C-SnO_2) samples.

The photocurrent density–voltage (*J–V*) characteristics of the DSSCs fabricated with different photoanodes are shown in Figure 3a and the corresponding PV parameters such as open-circuit voltage (V_{oc}), short-circuit current density (J_{sc}), fill factor (*FF*) and PCE have been summarized in Table 1. The control DSSC fabricated with TiO_2-only photoanode displayed a PCE of 5.10%. However, the AP-SnO_2-based DSSC exhibited a decreased PCE (4.47%) as compared to the TiO_2-only device (referred to here after as the 'control device'). This decrease in the cell performance after depositing AP-SnO_2 could be due to the fact that: (i) the non-crystalline SnO_2 showed insignificant light backscattering effect (see XRD pattern in Figure 2b); and/or (ii) hindrance of electrolyte infiltration due to strong aggregation of the SnO_2 particles (Figure 2c). By using the MW-SnO_2 structure in the photoanode, the fabricated DSSC showed an increased J_{sc} value and achieved a higher PCE (5.67%) than that of the control cell. This increase in the efficiency could be attributed to the reduced SnO_2 aggregation and possible improved backscattering. The DSSC fabricated with C-SnO_2 based photoanode exhibited a PCE of 6.32%, which is nearly 24% (relative) higher than that of the TiO_2-only photoanode. This high performance achieved for the C-SnO_2 sample when compared to the other SnO_2 based cells is due to the improved crystallinity of SnO_2 structure that significantly enhanced the light backscattering capability. On the basis of this high PCE, the C-SnO_2 sample was chosen for the fabrication of the DSSC devices and used for further investigations.

In order to determine the mechanism for enhanced PCE when using a TiO_2 + SnO_2 structure, the energy band levels of the components were compared (Figure 3b). It can be seen that the electrons at the SnO_2 conduction band cannot be transferred directly to the fluorine-doped tin oxide (FTO) electrode as SnO_2 was deposited on top of nanocrystalline TiO_2 and hence the SnO_2 layer is not physically (or electrically) connected to the FTO electrode. Therefore, these electrons can only be transferred to the external circuit through the TiO_2 layer. However, the conduction band of SnO_2 (–4.5 eV) is lower than that of TiO_2 (–4.26 eV);[17] such that electron transfer from the SnO_2 layer to the TiO_2 layer is thermodynamically unfavorable (see Figure 3b). In such case, extra dye loading on the SnO_2 and high electron mobility of SnO_2 cannot contribute to the efficiency enhancement of this class of DSSC device (TiO_2 + SnO_2 photoanode based). Indeed the enhancement in the performance for the calcined SnO_2 based DSSC should come from only the light backscattering effect of SnO_2.

Furthermore, the incident-photon-to-current conversion efficiency (IPCE) spectra offer detailed information on the light harvesting efficiency of the fabricated devices.[28, 29] Figure 3c illustrates the IPCE spectra of the DSSCs without and with SnO_2 layers as a function of wavelength. It should be noted that the IPCE spectra of the DSSCs were collected after the cell aging for around 12 days. As shown in Figure 3c, the IPCE of the DSSC fabricated with SnO_2 micro-rod based photoanode (TiO_2 + SnO_2) is higher than that of TiO_2-only photoanode cell over the entire wavelength region. The lack of wavelength dependence indicates the SnO_2 improves the performance of the DSSC without altering the internal mechanism, likely by increasing dye light absorption via light backscattering. Figure 4a shows the reflectance of SnO_2 films of various thicknesses. It is clear that the reflectance changes quite uniformly over the entire visible range confirming that improved light absorption, and hence higher IPCE, due to extra backscattering would be expected across the wavelengths measured as observed in Figure 3c.

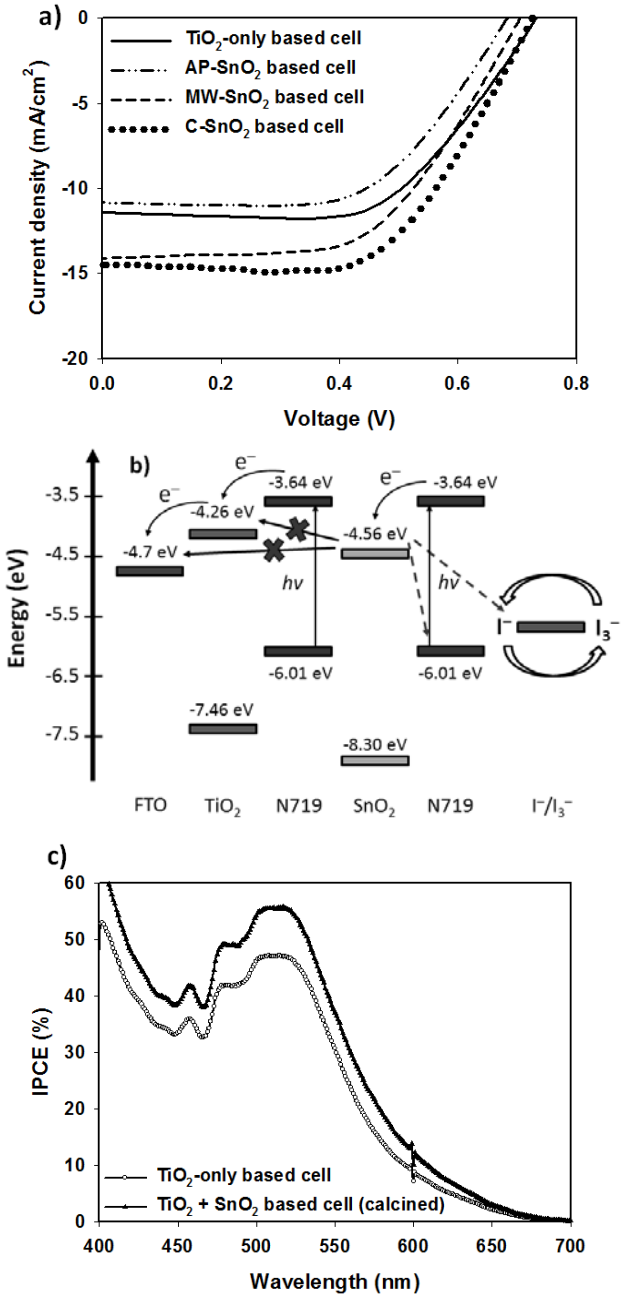

Figure 3 – (a) Photocurrent density–voltage (*J–V*) curves of DSSC devices fabricated with TiO_2-only and three samples based photoanodes, (b) possible energy level diagram for the TiO_2 + SnO_2 photoanode based DSSC and (c) IPCE of DSSCs based on TiO_2-only and TiO_2 + SnO_2 photoanodes.

Table 1. PV parameters and PCE (η) of DSSCs assembled with TiO_2-only (control device) photoanodes and three SnO_2-based photoanodes. The thicknesses of TiO_2 in the cells were ~15.5 µm. Average values and the standard deviations of the DSSCs are shown based on at least three cells for each device. Parameters of the best cells are also highlighted in **bold**.

Device	J_{sc} (mA cm^{-2})	V_{oc} (V)	*FF*	η (%)
TiO_2–only	**11.40**; 11.26 ± 0.40	**0.73**; 0.73 ± 0.01	**0.61**; 0.61 ± 0.02	**5.10**; 5.01 ± 0.12
AP-SnO_2	**10.84**; 10.27 ± 0.83	**0.69**; 0.69 ± 0.02	**0.60**; 0.59 ± 0.02	**4.47**; 4.29 ± 0.30
MW-SnO_2	**14.10**, 13.60 ± 0.98	**0.71**; 0.72 ± 0.01	**0.57**; 0.57 ± 0.02	**5.67**; 5.54 ± 0.13
C-SnO_2	**14.52**; 14.51 ± 0.43	**0.72**; 0.72 ± 0.01	**0.60**; 0.59 ± 0.01	**6.32**; 6.26 ± 0.11

In order to further confirm that the light backscattering effect is the main reason for the efficiency enhancement in SnO_2 enhanced DSSC system, PV characteristics of DSSCs fabricated with TiO_2-only and SnO_2 micro-rod based photoanodes have been measured using a mirror as a light reflector and their results are compared with the *J–V* measurement performed without mirror (Figure S2). Briefly, the mirror was placed at the back (counter electrode) of the device during the *J–V* scan. The PCE of the TiO_2-only photoanode based DSSC (5.10%) was increased to 5.90% with the use of mirror during the measurement, while almost no changes were observed with and without mirror for the cell based on SnO_2 layer. Importantly, PCE changes observed in the SnO_2-free photoanode based DSSC were mainly a result of the changes in the J_{sc} parameter. This result supports the aforementioned discussions and clearly suggests that the SnO_2 layer in such a device structure improves the DSSC performance due only to its light backscattering effect. A major advantage of this architecture is that the backscattering layer is placed between the light absorbing layer and the electrolyte and counter electrode. Both the electrolyte and counter electrode are opaque and therefore absorb some light, so simply placing a mirror behind the device does not achieve the same net effect as placing the SnO_2 light backscattering layer within the device, as can be seen by the fact that the measured PCE of the DSSC with the mirror (5.9%) does not reach that of the device with SnO_2 (6.4%).

Optimization of SnO_2 layer on the TiO_2 photoanode for DSSC performance

After confirming the light backscattering effect of C-SnO_2 layer, several investigations for the optimization of DSSC performance have been performed to maximize the PCE. In order to find an optimal SnO_2 layer on top of the TiO_2 layer, DSSC photoanodes were prepared by spin coating a SnO_2 colloidal solution onto the nanocrystalline TiO_2 film. The thickness of the SnO_2 layer was controlled by the number of spin coating cycles (varied from 0 to 12). SEM images of TiO_2 + SnO_2 films with different SnO_2 thickness are depicted in Figure S3. It can be observed from Figure S3 that the thicknesses of TiO_2 layers in all prepared films are consistent at 15.1–15.5 µm. Unexpectedly, the thickness of the SnO_2 layer does not appear to vary with the number of coating cycles. Instead, the SnO_2 layers in the films appear to become denser with increasing cycles (Figure S3).

To study the light backscattering efficiency of the prepared films, the reflectance of each film was characterized as a function of wavelength (from 400 nm to 800 nm), Figure 4a. The film prepared from a commercial TiO_2 paste (Ti-Nanoxide T/SP) supplied by Solaronix is highly transparent at wavelengths from 500 nm to 800 nm. It can be clearly seen that the reflectance (%) of the films increased with increasing the coating cycles of SnO_2 onto the TiO_2, indicating that the SnO_2 layer significantly improves the backscattering efficiency. As shown in Figure 4a, the reflectance of the film started to saturate (> 94%) after 8 spin coating cycles.

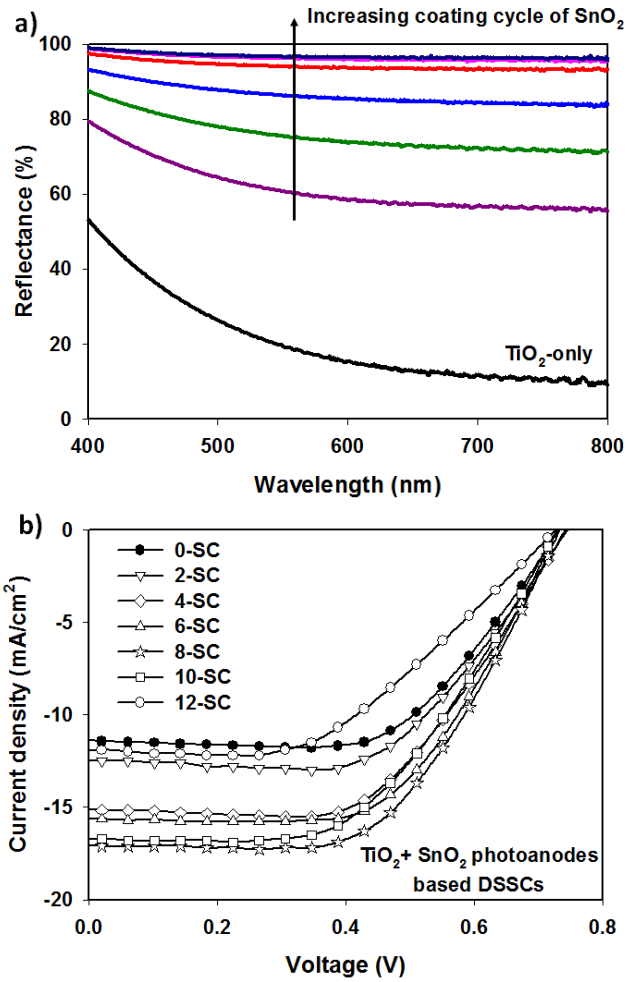

Figure 4 – (a) Reflectance spectra of the TiO_2 films with different coating cycles of SnO_2, and (b) *J–V* curves of DSSCs fabricated with different SnO_2 on TiO_2 photoanodes. Device number represents the spin coating (SC) cycle of SnO_2 onto ~15.5 µm thick TiO_2 layer.

The six photoanode films of different reflectance shown in Figure 4a were used in DSSC devices, denoted X-SC where the value of X indicates the number of spin coating cycles (e.g. the film prepared by spin coating SnO_2 for 2 cycles is denoted '2-SC'). The PV performances of the six DSSC devices (see Figure 4b) have been compared with the control device fabricated with TiO_2-only photoanode (0-SC).

The *J–V* characteristics of these DSSC devices are illustrated in Figure 4b. The detailed PV parameters such as J_{sc}, V_{oc}, *FF* and PCE are summarized in Table 2. The measured V_{oc} values of all DSSCs were similar at 0.73–0.74 V, indicating that the density of SnO_2 layer does not influence this parameter. This is reasonable since the V_{oc} in DSSCs is mainly determined by the energy difference between the conduction band of electron transporting material (TiO_2 in this device) and the potential energy of redox couple in the electrolyte (I^-/I_3^-). In contrast, several interesting changes in the J_{sc} and *FF* values were observed. As shown in Table 2, the control device showed a J_{sc} of 11.40 mA cm^{-2}. As compared to this J_{sc} value of 0-SC, continuous increases were observed until 8-SC. In particular, the J_{sc} value increased significantly from 11.40 mA cm^{-2} to 17.10 mA cm^{-2} for 8-SC due to the efficient light backscattering of SnO_2 layer in the cell. However, when SnO_2 layer becomes too dense (10-SC and 12-SC), the J_{sc} values of the DSSC drop significantly despite the photoanodes having high reflectance. We attribute this decrease in the J_{sc} to the limited infiltration of the electrolyte into the photoanode of the cell.

To confirm this explanation, a simple experiment was carried out by comparing electrolyte infiltration into the following two different spin coated SnO_2 films on FTO substrate: (i) 4 cycles (Figure S4a); and (ii) 12 cycles (Figure S4b). Briefly, two dummy cells were fabricated using the SnO_2 films. Then the same volume of electrolyte solution was injected into each cell via a vacuum filling method. Digital photographs (taken from the FTO side) of the SnO_2 films after electrolyte injection are shown in Figure S4a′ and S4b′. The electrolyte was well infiltrated into the SnO_2 film prepared with 4 spin coating cycles (Figure S4a′), while the dense SnO_2 film (12 spin coating cycles) showed little of the electrolyte at the bottom of the film clearly indicating poorer electrolyte diffusion into the denser film (Figure S4b′) which will lead to poorer cell performance. Therefore, it is clear that the dense SnO_2 films partially blocks the electrolyte infiltration into the nanocrystalline TiO_2 layers in our DSSCs and thus resulted in decreased J_{sc}. Indeed, the highest PCE was achieved for the 8-SC (8 spin coating cycles of SnO_2). In particular, the measured J_{sc}, V_{oc} and *FF* values for this DSSC (8-SC) were 17.10 mA cm^{-2}, 0.73 V and 0.57, respectively, yielding a PCE of 7.20%. Based on the achieved PCE results, 8 spin coating cycles produces the best solar cells and was further used for the fabrication of other DSSCs.

Table 2. PV parameters and PCE (η) of DSSCs fabricated with different SnO_2 on ~15.5 µm TiO_2 photoanodes. Reflectance (R, %) values at λ=520 nm (max IPCE (%) at this wavelength) are shown. Parameters of the best cells are also highlighted in **bold**.

Device	R (%) @ (520 nm)	J_{sc} (mA cm^{-2})	V_{oc} (V)	*FF*	η (%)
0-SC	23.0	**11.40**; 11.26 ± 0.40	**0.73**; 0.73 ± 0.01	**0.61**; 0.61 ± 0.02	**5.10**; 5.01 ± 0.12
2-SC	62.8	**12.44**; 12.26 ± 0.26	**0.74**; 0.72 ± 0.02	**0.59**; 0.60 ± 0.01	**5.50**; 5.31 ± 0.26
4-SC	76.8	**15.12**; 14.72 ± 0.55	**0.74**; 0.73 ± 0.01	**0.57**; 0.58 ± 0.02	**6.34**; 6.27 ± 0.11
6-SC	87.1	**15.63**; 15.70 ± 0.26	**0.73**; 0.73 ± 0.01	**0.59**; 0.56 ± 0.03	**6.73**; 6.43 ± 0.26
8-SC	94.4	**17.10**; 17.08 ± 0.05	**0.73**; 0.73 ± 0.005	**0.57**; 0.56 ± 0.01	**7.20**; 7.07 ± 0.13
10-SC	96.4	**16.77**; 16.40 ± 0.37	**0.73**; 0.72 ± 0.01	**0.53**; 0.54 ± 0.01	**6.45**; 6.41 ± 0.05
12-SC	96.9	**11.97**; 11.4 ± 1.07	**0.73**; 0.72 ± 0.01	**0.48**; 0.50 ± 0.03	**4.16**; 4.10 ± 0.10

Optimization of TiO_2 thickness in the photoanodes for DSSC performance

It is well established that the PV performance of DSSCs strongly depends on the thickness of the nanocrystalline TiO_2 layer. For instance, thick TiO_2 films provide higher absolute surface area for dye adsorption and demonstrate good charge generation; but they suffer from slow electron transport caused by a large number of grain boundaries. In contrast, poor charge generation rate caused by insufficient dye loading is the main issue of thin TiO_2 films, although they can rapidly transfer the electrons into the external circuit. It is worth noting that the light backscattering layer on top of thin nanocrystalline TiO_2 layer could enhance the light harvesting ability of the DSSC without altering the rapid electron transfer rate. To investigate this, six DSSC devices fabricated without and with SnO_2 backscattering layers on different thickness of TiO_2 layers were investigated. Cross sectional SEM images of the photoanodes prepared using 8 spin coating cycles of SnO_2 on top of TiO_2 layers with thicknesses of ~7.4 µm, ~10.8 µm and ~15.1 µm are illustrated in Figure 5a, Figure 5b and Figure 5c, respectively. The corresponding *J–V* characteristics and PCEs of these DSSCs are shown in Figure 5a′, Figure 5b′ and Figure 5c′. Among the three SnO_2-free photoanodes based DSSCs; the cell fabricated with ~10.8 µm thick nanocrystalline TiO_2 film exhibited the highest PCE (5.60%). It can be clearly observed from Figure 5 that the use of SnO_2 light backscattering layers improved the cell performance of all three TiO_2 photoanodes. Indeed, the SnO_2 layer on ~10.8 µm thick TiO_2 film showed an impressive enhancement (~38% (relative) increase) in the DSSC efficiency as compared to the same thickness TiO_2-only photoanode based cell. Particularly, this best DSSC achieved a PCE of 7.80%.

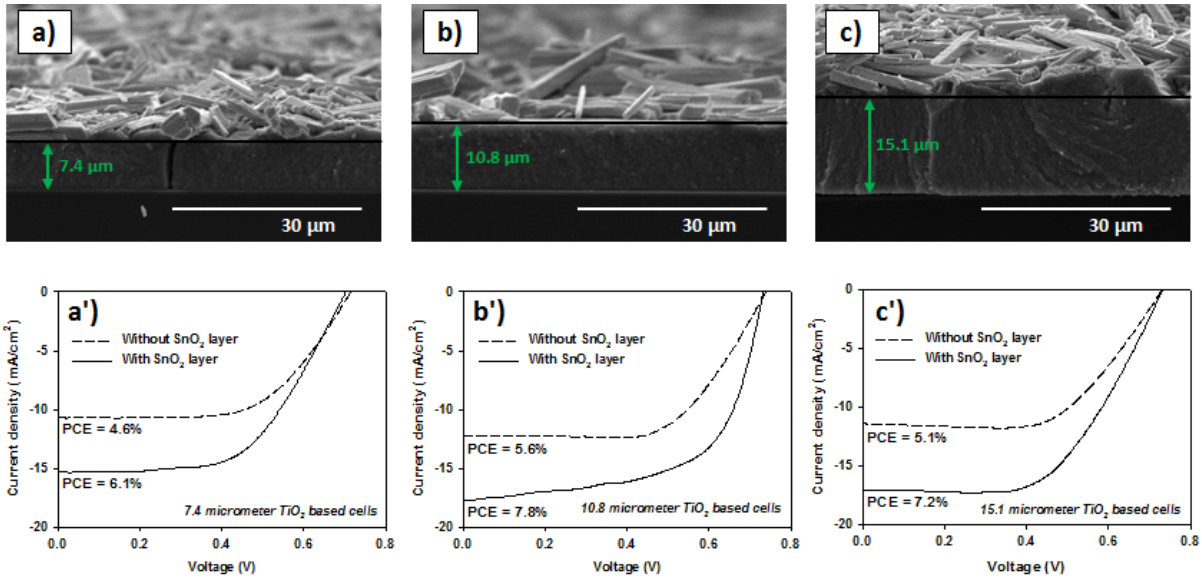

Figure 5 – Cross sectional SEM image of SnO_2 deposited (8 spin coating cycles) on (a) 7.4 µm, (b) 10.8 µm and (c) 15.1 µm TiO_2 films. *J–V* curves of DSSCs fabricated without and with SnO_2 layers on (a) 7.4 µm, (b) 10.8 µm and (c) 15.1 µm TiO_2 photoanodes. Highest PCEs of the cells are reported here.

Overall, a noticeable feature from the *J–V* characteristics of all devices made without and with SnO_2 is that the *FF* values of the DSSCs decreased after depositing SnO_2 on top of the nanocrystalline TiO_2 layers. This can be associated with the energy level alignment of TiO_2 and SnO_2. As shown in Figure 3b, the photoexcited electrons can be injected into both TiO_2 and SnO_2 as dye molecules are adsorbed on both layers. However, the electrons at the SnO_2 conduction band cannot be transferred to the TiO_2 and FTO (external circuit) as the conduction band of SnO_2 (-4.50 eV) is lower than that of TiO_2 (-4.26 eV). This unsuccessful electron transfer between the SnO_2 and TiO_2 must lead to some charge recombination between the photoexcited electrons and the oxidized electrolyte species, thus resulting in decreased *FF* value (see red dash lines in Figure 3b).

It can be seen from Figure 6 that the PCE enhancements observed for the SnO_2 deposited TiO_2 photoanodes based DSSCs are comparable and/or higher than that achieved by other light backscattering layers. The TiO_2 backscattering layers have a dual action; namely 1) backscattering light and 2) adsorption of extra dye which can create extra electrons. Thus, it is not surprising that some TiO_2 systems show better performance than the SnO_2 systems. The fact that the SnO_2 systems perform as well as they do indicate just how effective the backscattering is in these systems. Additionally, the possibility that significant PCE enhancement might be achieved by tuning the conduction band of SnO_2 by doping with other species points to interesting future work.

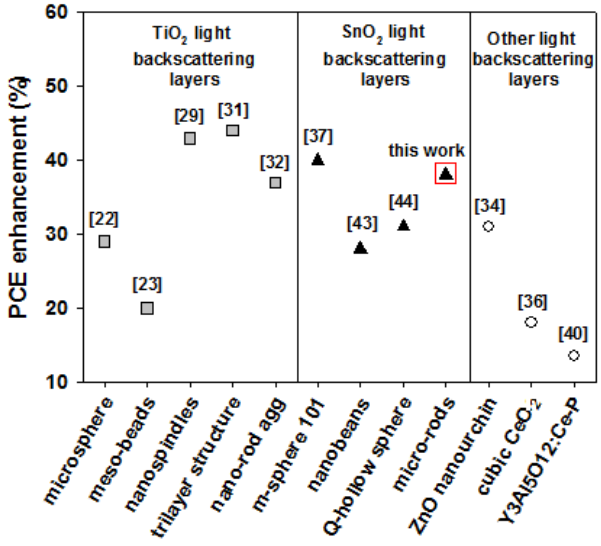

Figure 6 – PCE enhancements of DSSCs in the presence of different light backscattering layers. The numbers are the reference numbers. PCE enhancements are calculated based on the best PCE value of DSSCs fabricated with backscattering layer and the control TiO_2-only based cell.

Conclusions

SnO_2 micro-rods have been synthesized and employed as a light backscattering layer for TiO_2 photoanode based DSSCs. The detailed analysis with XRD, FTIR and SEM suggests that the crystallinity of SnO_2 structure is of great importance for the light backscattering capability of SnO_2 layer to enhance the DSSC efficiency. After optimizing the thickness of SnO_2 and TiO_2 layers, PCE of the cell was significantly improved to 7.80%,

demonstrating a ~38% enhancement in the efficiency when compared to TiO_2-only photoanode based DSSC (5.6%). We confirmed that this significant improvement in the efficiency is due mainly to the efficient light backscattering capability of SnO_2.

Experimental Section

Materials: Unless otherwise stated, all chemicals were purchased from Sigma-Aldrich and used without further purification. Tin (II) chloride dihydrate ($SnCl_2{\cdot}2H_2O$) powder (>99% purity, Merck) was used as a starting material. FTO coated glass electrode with a sheet resistance (R_s) of ~12 Ω/□ (TCO30-8), TiO_2 paste (Ti-Nanoxide T/SP), Ruthenizer 535-bisTBA (N719 dye), iodide/tri-iodide electrolyte (Iodolyte Z-50), DuPont Surlyn® (Meltonix 1170-60) and Platinum catalyst (Platisol T, HS Code. 7110.1900) were purchased from Solaronix, Switzerland.

Synthesis of SnO_2 structures: Three different SnO_2 structures were synthesized from $SnCl_2{\cdot}2H_2O$. In a typical process, 1.5 g of $SnCl_2{\cdot}2H_2O$ powder was added into 200 mL of 0.02M HCl solution, followed by stirring the solution for 45 min in air. Under these conditions, precipitation of SnO_2 rods is achieved. 50 mL of the resultant product was dried in an oven at 80°C after complete washing with DI water. The dried sample is called "as prepared" SnO_2 (AP-SnO_2). The remaining solution was then reacted using a microwave technique (StartSYNTH Microwave Synthesis Labstation, Milestone s.r.l) for 5 min under 600 W power. The temperature was controlled at 90°C during the microwave treatment. The obtained precipitate was washed several times with DI water and then dried overnight at 80°C. The resultant product is termed "microwaved" SnO_2 (MW-SnO_2). Then the MW-SnO_2 sample was calcined using a muffle furnace at 500°C for 3 h in air. The final product is named "calcined" SnO_2 (C-SnO_2) sample.

DSSC fabrication: FTO coated substrates were cleaned by a detergent (Pyroneg) followed by washing with acetone, ethanol and Milli-Q water under ultrasonication for 10 min each and subsequently dried with a nitrogen gas.[47] The cleaned FTO electrodes were soaked in a 40 mM $TiCl_4$ aqueous solution for 30 min at 70°C. Nanocrystalline TiO_2 films (5 x 5 mm) were prepared from a commercial TiO_2 paste (Ti-Nanoxide T/SP, Solaronix) by doctor blading technique. For the fabrication of different SnO_2 (AP-SnO_2, MW-SnO_2, C-SnO_2 and spin coating cycles) based DSSCs, the thicknesses of the bottom TiO_2 layers (15.1 µm–15.5 µm) were obtained by using two layers of adhesive scotch tape (Magic™ *Tape*, 3M). 7.4 µm TiO_2 film was prepared using only one layer of 3M tape. Alternatively, for the preparation of 10.8 µm TiO_2 film, two layers of scotch tape (general purpose tape, *OfficeMax*) were used. After the deposition of TiO_2 paste onto the FTO substrates, TiO_2 films were gradually heated under an air flow at 125°C for 5 min, 325°C for 5 min, at 375°C for 5 min and at 450°C for 30 min, followed by cooling to ~50°C. TiO_2 films were then immersed in 40 mM $TiCl_4$ solution at 70°C for 30 min, then sintered at 450°C for 30 min. After cooling to room temperature, SnO_2 backscattering layers were deposited on top of nanocrystalline TiO_2 layers.

Viscous SnO_2 pastes were prepared from AP-SnO_2, MW-SnO_2 and C-SnO_2 samples according to the established procedures described in the literature.[47] As for the preparation of AP-SnO_2, MW-SnO_2 and C-SnO_2 based photoanodes, the SnO_2 pastes were deposited on TiO_2 coated FTO substrate by doctor blading method using 3 layers of adhesive tape (3M). During doctor blading of SnO_2 paste, adhesive tapes covered the FTO electrode by leaving TiO_2 film; so that the SnO_2 layer overlaps with TiO_2 layer. To optimize the thickness of SnO_2 layer in photoanodes, the previously prepared SnO_2 paste (C-SnO_2 was chosen) were diluted with ethanol (1:4 weight ratio) to obtain a SnO_2 colloidal solution. Then the SnO_2 solution was deposited onto the nanocrystalline TiO_2 by spin coating at 2000 rpm for 30 s. Different spin coating cycles (0–12 cycles) were used to control the density of the SnO_2 layers. Between each spin coating cycle, the films were dried at 150°C in air.

The various photoanodes were sintered at 500°C for 1 h and after cooling to ~50°C were immersed into 0.5 mM N719 dye in an ethanol solution for 18 h at room temperature. Afterwards, the photoanodes were washed with ethanol to remove non-adsorbed dye from the films. Platinum (Pt) counter electrodes were prepared by coating liquid Pt precursor (Platisol T, Solaronix), used as received, onto FTO substrates using a brush-painting method followed by heating at 450°C for 20 min on a hot plate in air The dye-loaded photoanode and Pt counter electrode were assembled into a sealed sandwich-type cell, with a 60 µm thick hot-melt sealing Surlyn between each layer. The electrolyte solution, Iodolyte Z-50, was introduced into the cell via a vacuum-filling method through an injection hole on the counter electrode side. Finally, the hole was sealed with Surlyn and a microscope glass cover.

Measurement and Characterization: SEM images were obtained using an Inspect F50 SEM (FEI) with accelerating voltage of 10 kV. The thicknesses of the films were measured from the cross sectional SEM images. XRD patterns were recorded on a powder X-ray diffractometer at 40 kV and 15 mA in the range of 2θ = 20–80° using Cu Kα radiation (Model Miniflex 600, Rigaku, Japan). ATR-FTIR spectra were acquired over a wavenumber range of 4000-500 cm^{-1} in transmission mode using a Frontier FTIR spectrometer (Perkin Elmer, USA) with a germanium crystal. The reflectances of the films on FTO substrates were characterized using a Varian Cary 50G UV-vis Spectrophotometer at wavelengths ranging from 400 to 800 nm. The *J–V* characteristics (J_{sc}, V_{oc}, *FF* and η) were studied using a Keithley 2400 SMU instrument and recorded using a custom LabView Virtual Instrument program. A standard silicon test cell with NIST-traceable certification was used to calibrate the power density as 100 mW cm^{-2} at the sample plane of the collimated xenon-arc light source, which was passed through an AM 1.5G filter. The active area of each device was 0.25 cm^2. The *J-V* curves were measured in the air through reverse-scan direction from 1 V to -1 V. The PCE, η, was calculated from the ratio of output power, P_{max}, to the power incident per unit area on the solar device (P_{in}). P_{max} and therefore, PCE was calculated from following equation:

$$\eta = \frac{P_{max}}{P_{in}} = \frac{J_{SC} \times V_{OC} \times FF}{P_{in}}$$

For analysis of mirror effect on the PV characteristics of DSSCs, the mirror was placed at the back (counter electrode) of the device during the *J–V* scan. IPCE measurements as a function of wavelength ranging from 400 nm to 700 nm were taken by passing chopped light from a Xenon source through a monochromator and onto the devices.

Acknowledgements

The support of the Australian Research Council Discovery Program (DP130101714) is gratefully acknowledged. Munkhbayar Batmunkh acknowledges International Postgraduate Research Scholarship (IPRS) and Australian Postgraduate Award (APA) for their financial support during his study in Australia. We acknowledge the use of South Australian node of the Australian Microscopy & Microanalysis Research Facility (AMMRF) at Flinders University.

Keywords: Photovoltaic • Dye-sensitized solar cells • Photoanode • Tin oxide • Light scattering

[1] R. E. Smalley *MRS Bulletin*. **2005**, 30, 412-417.
[2] H. S. Jung, N.-G. Park *Small*. **2015**, 11, 10-25.
[3] M. Batmunkh, M. J. Biggs, J. G. Shapter *Advanced Science*. **2015**, 2, 1400025.
[4] W. S. Yang, J. H. Noh, N. J. Jeon, Y. C. Kim, S. Ryu, J. Seo, S. I. Seok *Science*. **2015**, 348, 1234-1237.
[5] K. Kakiage, Y. Aoyama, T. Yano, K. Oya, J.-i. Fujisawa, M. Hanaya *Chemical Communications*. **2015**, 51, 15894-15897.
[6] M. Ye, X. Wen, M. Wang, J. Iocozzia, N. Zhang, C. Lin, Z. Lin *Materials Today*. **2015**, 18, 155-162.
[7] M. Batmunkh, M. J. Biggs, J. G. Shapter *Small*. **2015**, 11, 2963-2989.
[8] F. Bella, C. Gerbaldi, C. Barolo, M. Gratzel *Chemical Society Reviews*. **2015**, 44, 3431-3473.
[9] J. Wu, Z. Lan, J. Lin, M. Huang, Y. Huang, L. Fan, G. Luo *Chemical Reviews*. **2015**, 115, 2136-2173.
[10] G. Hashmi, K. Miettunen, T. Peltola, J. Halme, I. Asghar, K. Aitola, M. Toivola, P. Lund *Renewable and Sustainable Energy Reviews*. **2011**, 15, 3717-3732.
[11] Q. Zhang, T. P. Chou, B. Russo, S. A. Jenekhe, G. Cao *Angewandte Chemie International Edition*. **2008**, 47, 2402-2406.
[12] Q. Zhang, G. Cao *Nano Today*. **2011**, 6, 91-109.
[13] Q. Zhang, K. Park, J. Xi, D. Myers, G. Cao *Advanced Energy Materials*. **2011**, 1, 988-1001.
[14] J. Kim, J. K. Koh, B. Kim, J. H. Kim, E. Kim *Angewandte Chemie International Edition*. **2012**, 51, 6864-6869.
[15] J. Na, J. Kim, C. Park, E. Kim *RSC Advances*. **2014**, 4, 44555-44562.
[16] J. Na, Y. Kim, C. Park, E. Kim *NPG Asia Mater*. **2015**, 7, e217.
[17] A. Thapa, J. Zai, H. Elbohy, P. Poudel, N. Adhikari, X. Qian, Q. Qiao *Nano Res.* **2014**, 7, 1154-1163.
[18] J. Lin, Y.-U. Heo, A. Nattestad, Z. Sun, L. Wang, J. H. Kim, S. X. Dou *Scientific Reports*. **2014**, 4, 5769.
[19] J. Lin, Y.-U. Heo, A. Nattestad, Y. Yamauchi, S. X. Dou, J. H. Kim *Electrochimica Acta*. **2015**, 153, 393-398.
[20] H. J. Koo, Y. J. Kim, Y. H. Lee, W. I. Lee, K. Kim, N. G. Park *Advanced Materials*. **2008**, 20, 195-199.
[21] K. Li, J. Xu, W. Shi, Y. Wang, T. Peng *Journal of Materials Chemistry A*. **2014**, 2, 1886-1896.
[22] J. Feng, Y. Hong, J. Zhang, P. Wang, Z. Hu, Q. Wang, L. Han, Y. Zhu *Journal of Materials Chemistry A*. **2014**, 2, 1502-1508.
[23] F. Huang, D. Chen, X. L. Zhang, R. A. Caruso, Y.-B. Cheng *Advanced Functional Materials*. **2010**, 20, 1301-1305.
[24] D. Chen, F. Huang, Y.-B. Cheng, R. A. Caruso *Advanced Materials*. **2009**, 21, 2206-2210.
[25] Z. Sun, J. H. Kim, Y. Zhao, D. Attard, S. X. Dou *Chemical Communications*. **2013**, 49, 966-968.
[26] J.-Y. Liao, B.-X. Lei, D.-B. Kuang, C.-Y. Su *Energy & Environmental Science*. **2011**, 4, 4079-4085.
[27] J. Lin, A. Nattestad, H. Yu, Y. Bai, L. Wang, S. X. Dou, J. H. Kim *Journal of Materials Chemistry A*. **2014**, 2, 8902-8909.
[28] K. Yan, Y. Qiu, W. Chen, M. Zhang, S. Yang *Energy & Environmental Science*. **2011**, 4, 2168-2176.
[29] Y. Qiu, W. Chen, S. Yang *Angewandte Chemie International Edition*. **2010**, 49, 3675-3679.
[30] K. Fan, W. Zhang, T. Peng, J. Chen, F. Yang *The Journal of Physical Chemistry C*. **2011**, 115, 17213-17219.
[31] M. Liu, H. Wang, C. Yan, G. Will, J. Bell *Applied Physics Letters*. **2011**, 98, 133113.
[32] Z.-H. Liu, X.-J. Su, G.-L. Hou, S. Bi, Z. Xiao, H.-P. Jia *Journal of Power Sources*. **2012**, 218, 280-285.
[33] Y.-Z. Zheng, X. Tao, L.-X. Wang, H. Xu, Q. Hou, W.-L. Zhou, J.-F. Chen *Chemistry of Materials*. **2010**, 22, 928-934.
[34] Y.-Z. Zheng, H. Ding, Y. Liu, X. Tao, G. Cao, J.-F. Chen *Journal of Power Sources*. **2014**, 254, 153-160.
[35] X.-H. Lu, Y.-Z. Zheng, S.-Q. Bi, Y. Wang, X. Tao, L. Dai, J.-F. Chen *Advanced Energy Materials*. **2014**, 4, 1301802.
[36] H. Yu, Y. Bai, X. Zong, F. Tang, G. Q. M. Lu, L. Wang *Chemical Communications*. **2012**, 48, 7386-7388.
[37] W. Peng, X. Yang, Z. Chen, J. Zhang, H. Chen, K. Zhang, L. Han *ChemSusChem*. **2014**, 7, 172-178.
[38] Y.-F. Wang, K.-N. Li, W.-Q. Wu, Y.-F. Xu, H.-Y. Chen, C.-Y. Su, D.-B. Kuang *RSC Advances*. **2013**, 3, 13804-13810.
[39] J. Gong, H. Qiao, S. Sigdel, H. Elbohy, N. Adhikari, Z. Zhou, K. Sumathy, Q. Wei, Q. Qiao *AIP Advances*. **2015**, 5, 067134.
[40] G. Zhu, X. Wang, H. Li, L. Pan, H. Sun, X. Liu, T. Lv, Z. Sun *Chemical Communications*. **2012**, 48, 958-960.
[41] J. Qian, P. Liu, Y. Xiao, Y. Jiang, Y. Cao, X. Ai, H. Yang *Advanced Materials*. **2009**, 21, 3663-3667.
[42] J. Chen, C. Li, F. Xu, Y. Zhou, W. Lei, L. Sun, Y. Zhang *RSC Advances*. **2012**, 2, 7384-7387.
[43] C.-L. Wang, J.-Y. Liao, Y. Zhao, A. Manthiram *Chemical Communications*. **2015**, 51, 2848-2850.
[44] Z. Dong, H. Ren, C. M. Hessel, J. Wang, R. Yu, Q. Jin, M. Yang, Z. Hu, Y. Chen, Z. Tang, H. Zhao, D. Wang *Advanced Materials*. **2014**, 26, 905-909.
[45] F. Gu, S. F. Wang, M. K. Lü, G. J. Zhou, D. Xu, D. R. Yuan *The Journal of Physical Chemistry B*. **2004**, 108, 8119-8123.
[46] A. P. Alivisatos *The Journal of Physical Chemistry*. **1996**, 100, 13226-13239.
[47] S. Ito, P. Chen, P. Comte, M. K. Nazeeruddin, P. Liska, P. Péchy, M. Grätzel *Progress in Photovoltaics: Research and Applications*. **2007**, 15, 603-612.

Photovoltaic cells based on SnO_2 structures.

FULL PAPER

SnO_2 microstructures have been employed as a light backscattering layer for TiO_2 photoanode based dye-sensitized solar cells. SnO_2 structures with high-crystallinity are shown to have a very strong light backscattering capability and significantly enhance the efficiency of photovoltaic cell.

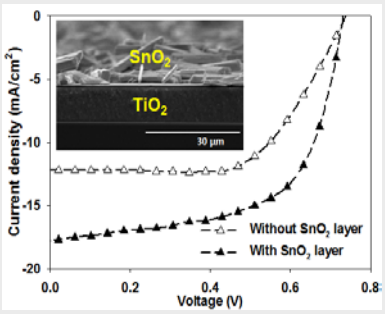

*Munkhbayar Batmunkh, Mahnaz Dadkhah, Cameron J. Shearer, Mark J. Biggs and Joseph G. Shapter**

Page No. – Page No.

SnO_2 Light Scattering Layer for TiO_2 Photoanode in Dye-Sensitized Solar Cells

Supporting Information

SnO_2 Light Scattering Layer for TiO_2 Photoanode in Dye-Sensitized Solar Cells

Munkhbayar Batmunkh,[a,b] Mahnaz Dadkhah,[b] Cameron J. Shearer,[b] Mark J. Biggs,[a,c] and Joseph G. Shapter [b]*

[a] *School of Chemical Engineering, The University of Adelaide, Adelaide, SA 5005, Australia*

[b] *School of Chemical and Physical Sciences, Flinders University Bedford Park, GPO Box 2100, Adelaide, SA 5001, Australia*

[c] *School of Science, Loughborough University, Loughborough, Leicestershire LE11 3TU, UK*

Corresponding author: joe.shapter@flinders.edu.au

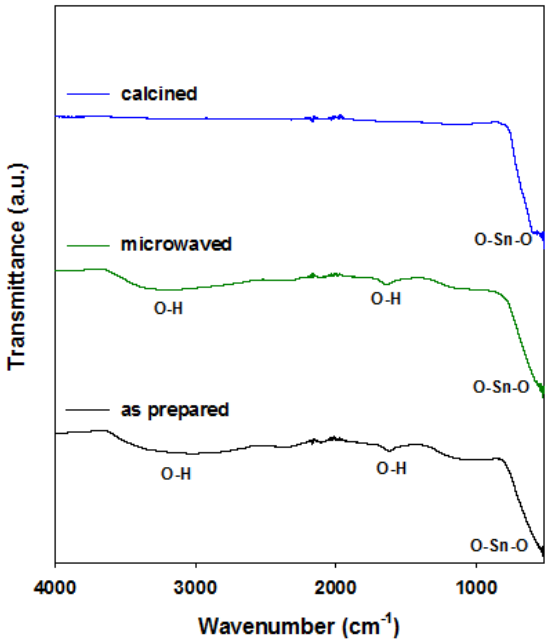

Figure S1 – ATR-FTIR spectra of the prepared samples.

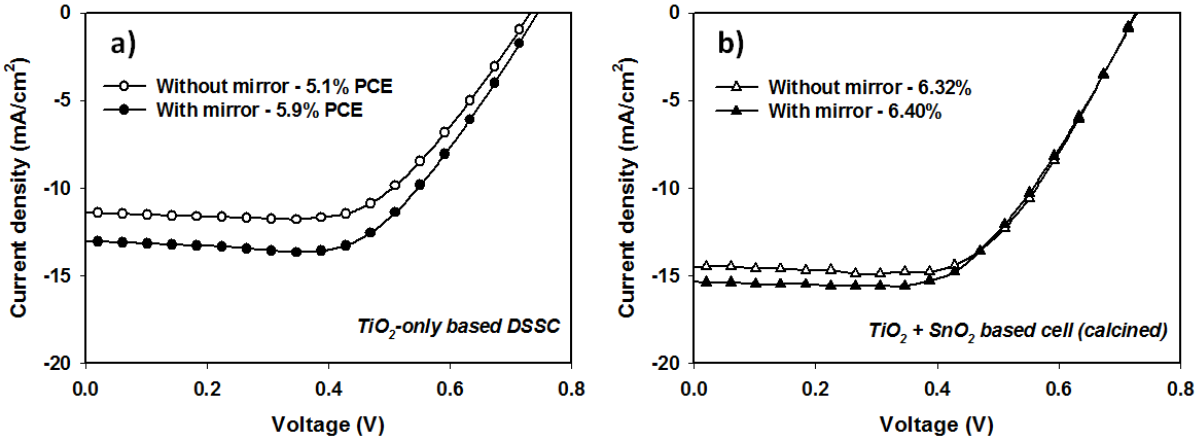

Figure S2 – Effect of mirror on the performance of DSSCs fabricated with (a) TiO_2-only photoanode and (b) TiO_2 + SnO_2 photoanode.

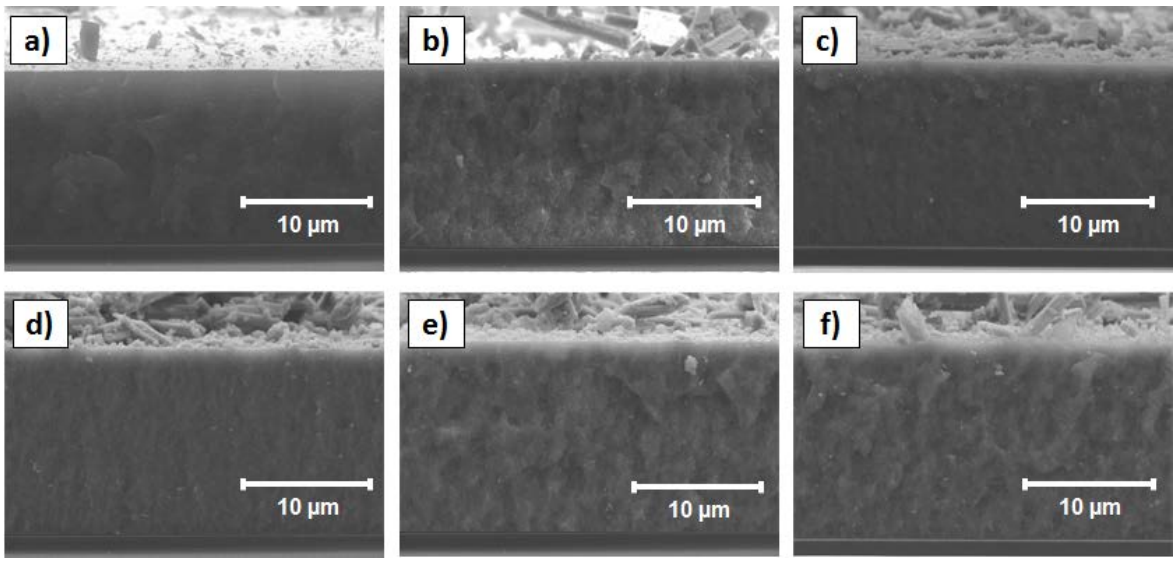

Figure S3 – SEM image of SnO_2 microstructure on nanocrystalline TiO_2. SnO_2 was deposited by spin coating a colloidal solution of SnO_2 for (a) 2 cycles, (b) 4 cycles, (c) 6 cycles, (d) 8 cycles, (e) 10 cycles and (f) 12 cycles.

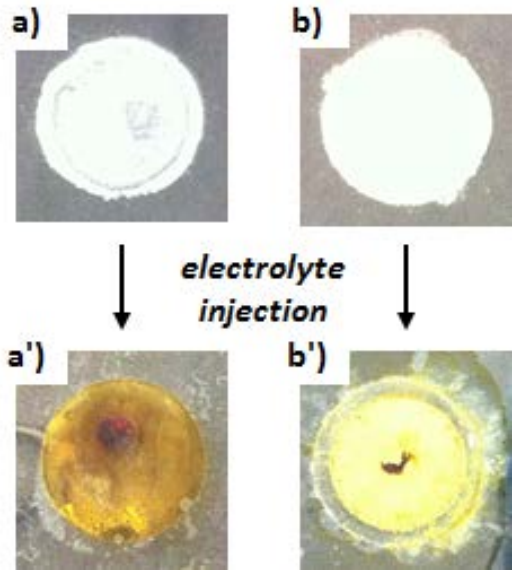

Figure S4 – Digital photograph of (a) 4 cycles (less dense) and (b) 12 cycles (highly dense) spin coated SnO_2 films before (top) and after (bottom) electrolyte injection.